Journal of Medicinal Chemistry

ARTICLE

pubs.acs.org/jmc

Development of the Fluorescent Biosensor *h*Calmodulin (*h*CaM)L39C-*monobromobimane*(*mBBr*)/V91C-*mBBr*, a Novel Tool for Discovering New Calmodulin Inhibitors and Detecting Calcium

Martín González-Andrade,[†] José Rivera-Chávez,[†] Alejandro Sosa-Peinado,[‡] Mario Figueroa,[†] Rogelio Rodríguez-Sotres,[†] and Rachel Mata*[,†]

[†]Facultad de Química, Universidad Nacional Autónoma de México, México DF 04510, México

[‡]Facultad de Medicina, Universidad Nacional Autónoma de México, México DF 04510, México

Supporting Information

ABSTRACT: A novel, sensible, and specific fluorescent biosensor of human calmodulin (*h*CaM), namely *h*CaM L39C-*mBBr*/V91C-*mBBr*, was constructed. The biosensor was useful for detecting ligands with opposing fluorescent signals, calcium ions (Ca^{2+}) and CaM inhibitors in solution. Thus, the device was successfully applied to analyze the allosteric effect of Ca^{2+} on trifluoroperazine (**TFP**) binding to CaM (Ca^{2+} K_d = 0.24 μM ± 0.03 with a stoichiometry 4.10 ± 0.15; **TFP** K_d ~ 5.74−0.53 μM depending on the degree of saturation of Ca^{2+}, with a stoichiometry of 2:1). In addition, it was suitable for discovering additional xanthones (**5**, **6**, and **8**) with anti-CaM properties from the fungus *Emericella* 25379. The affinity of **1**−**5**, **7**, and **8** for the complex $(Ca^{2+})_4$-CaM was excellent because their experimental K_ds were in the nM range (4−498 nM). Docking analysis predicted that **1**−**8** bind to CaM at sites I, III, and IV as does **TFP**.

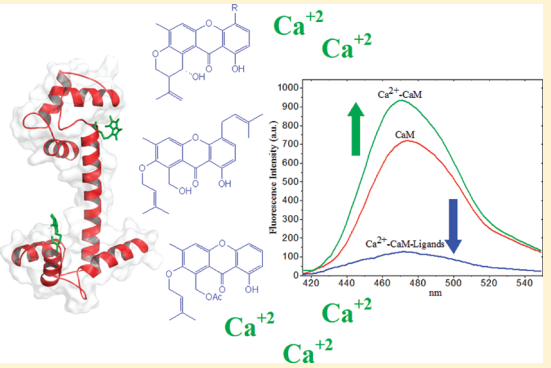

INTRODUCTION

The discovery of new chemical entities (synthetic, natural product, or biotechnological) with pharmacological properties has been a trend in pharmaceutical research in recent years. For this reason, the development of modern methods, including biosensors, for pharmacological screening is very important. A biosensor is a device that consists of a biological recognition system, often called a bioreceptor, and a physical transducer which allows the conversion of a biological response into a measurable effect, for example, electric or fluorescence signals.[1] This molecular target usually utilizes a biochemical mechanism for recognition and is the key to the specificity of a biosensor. Many bioreceptors have been used to build biosensors valuable for monitoring different types of analytes. Proteins, including enzymes, antibody, or ion channels, are often chosen as bioreceptors due to their specific binding capabilities.

One promising biological molecular species useful for building biosensors is the protein calmodulin (CaM), the primary transducer of calcium (Ca^{2+})-mediated signals in eukaryotes.[2] According to a resolved crystal structure, CaM is dumbbell-shaped protein with two domains separated by a long central helix; each domain contains two EF hand Ca^{2+}-binding loops, which tightly bind a Ca^{2+} ion each.[2]

CaM is involved in several cellular physiological processes, such as gene regulation, protein synthesis, fast axonal transport, smooth muscle contraction, secretion, growth, organelle tubulation, ion channel function, cell motility, and chemotaxis, to mention a few. Consequently, CaM has been also implicated in a variety of degenerative diseases processes such as inflammation, short-term memory, cancer, viral penetration, and immune response.[3−6] CaM controls all these processes, physiological or pathophysiological, through the modulation of at least 100 different proteins and CaM-dependent enzymes like calmodulin-sensitive *c*AMP phosphodiesterase (PDE1), nitric oxide synthases, adenylate cyclase, several kinases, calcium-ATPase pumps, ion channels, phosphatases as well as cytoskeletal structural proteins, among the most important.[7,8] Altogether, this information makes CaM an attractive bioreceptor for building biosensors suitable for the discovery of CaM ligands useful as new drugs or research tools to fully understand physiological CaM mediated processes.

To build a CaM biosensor, the transduction can be accomplished via different methods. However, fluorescence-based methods, including fluorescence resonance energy and extrinsic fluorescence, are the most popular.[9] The fluorescence-based methods are highly specific, low-cost, selective, and have short reaction times, although sometimes the preparation of the sensing element can be laborious. One of the most used procedures involves the

Received: February 15, 2011
Published: April 15, 2011

covalent attachment to CaM of a thiol-reactive fluorophore strategically located using site-directed mutagenesis and site-specific fluorescent labeling (Figure 1). When placed at an appropriate location, the probe makes it possible to correlate the conformational changes with ligand binding through the changes in the emission properties of the labeled proteins. In this regard, we have previously reported a CaM biosensor (*h*CaM M124C-*mBBr*), which was useful for detecting CaM inhibitors binding to the same region as trifluoroperazine (**TFP**) and other classical inhibitors.[10] This device possesses a unique cysteine (Cys) residue at position 124 chemically modified by attaching the fluorophore monobromobimane (*mBBr*). The fluorophore-labeled protein exhibited stability and functionality to the activation of CaM-sensitive *c*AMP phosphodiesterase (PDE1) similar to those of the wild-type *h*CaM. Herein, we report the design, production, and characterization of a sensitive and versatile fluorescent biosensor of human CaM (*h*CaM), namely *h*CaM L39C-*mBBr*/V91C-*mBBr*. This new tool was efficiently used to analyze the allosteric effect of calcium on **TFP** binding to CaM and to discover additional CaM inhibitors from the fungus *Emericella* 25379. As previously demonstrated, this fungal species biosynthesizes prenylated xanthones which inhibited the ability of CaM to activate sensitive CaM-dependent PDE1.[11] In addition, other investigations have shown that these type of metabolites displayed potential antihypertensive, antioxidative, antithrombotic, and antitumoral activities.[11−13]

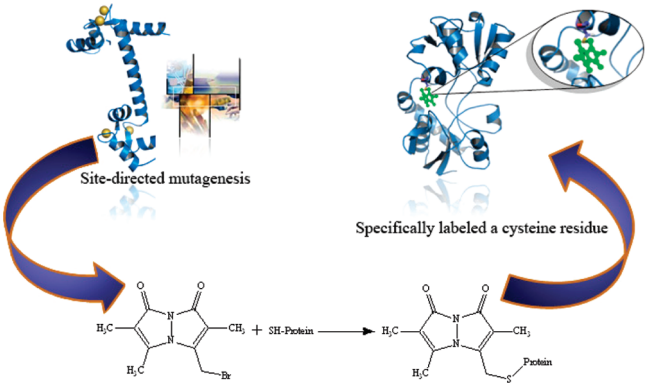

Figure 1. General strategy in the construction of the biosensors, using site-directed mutagenesis and site-specific fluorescent labeling, for the construction of biosensors.

RESULTS AND DISCUSSION

Design of Biosensor *h*CaM L39C-*mBBr*/V91C-*mBBr*. Figure 1 summarizes the general strategy followed to build *h*CaM L39C-*mBBr*/V91C-*mBBr*, which comprised site-directed mutagenesis for replacing the strategic residues Leu39 and Val91 by Cys followed by specific labeling of the thiol-reactive group with the fluorophore *mBBr*. These positions were selected for labeling considering that residues 39 and 91 of CaM are in an accessible surface area (ASA ≥ 40 Å^2), are not involved in calcium binding, and are located nearby to the regions where classical CaM inhibitors interact. Furthermore, in the free ligand conformation of the protein, the linear distance between the thiol groups of the cysteine residues at positions 39 and 91 (Cys39SG and Cys91SG) was 28.88 Å and in the complex $(Ca^{2+})_4$-*h*CaM L39C-*mBBr*/*V91C-mBBr*-**TFP** was 3.26 Å (Figure 2). The approximation of the fluorescent probes to each other, upon interaction of *h*CaM L39C-*mBBr*/V91C-*mBBr* with a ligand generates a strong fluorescent signal, making this new device useful as biological recognition system. Finally, both selected residues are part of the α-helice structure of CaM, thus minimizing potential structural changes.[14]

Production of the *h*CaM L39C-*mBBr*/V91C-*mBBr*. *hCaM L39C/V91C* was built from the gene *CALM1* (human phosphorylase kinase, δ) which encodes for *h*CaM; the gene was introduced in an overexpression vector pET (pET12b-CaM); site-directed

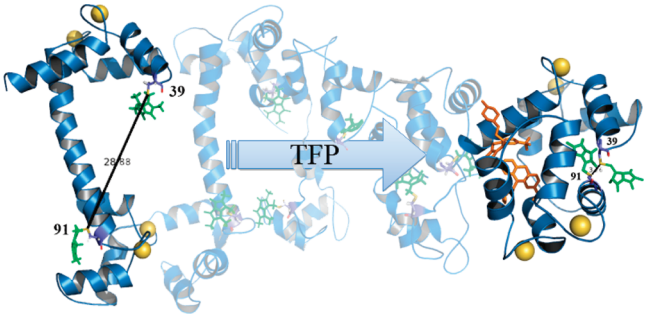

Figure 2. Structural model of *h*CaM L39C-*mBBr*/V91C-*mBBr* in absence (left) and presence (right) of the inhibitor **TFP**. The black straight lines show the linear distance between the thiol groups of cysteine residues at positions 39 and 91 (Cys39SG and Cys91SG) in the open (28.88 Å) and closed conformation 3.26 Å. The structures were drawn using PyMOL.[32]

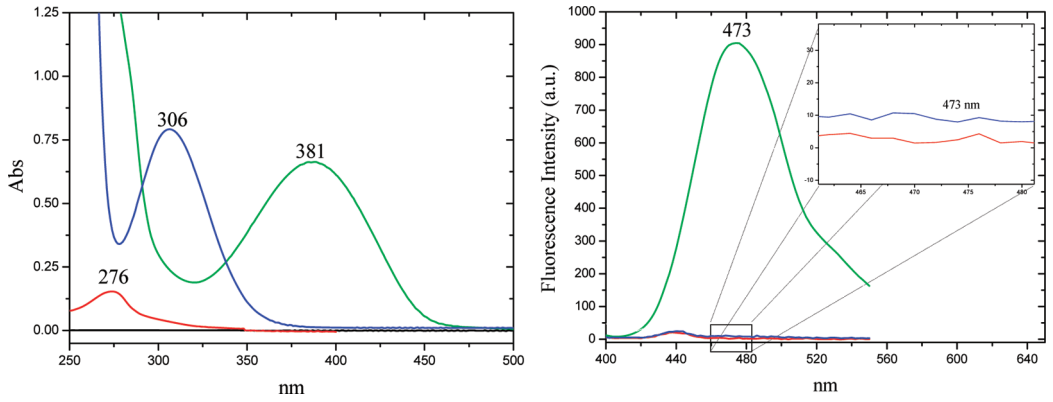

Figure 3. Absorption and fluorescence spectra of the CaM wild-type (1 μM), *h*CaM L39C-*mBBr*/V91C-*mBBr* (1 μM), and **TFP** (100 μM) in potassium acetate buffer (pH 5.5), at 37 °C. The left panel shows the absorption spectra of CaM wild-type (red line) and *h*CaM L39C-*mBBr*/V91C-*mBBr* (green line), inhibitor TFP (blue line), and the buffer alone (−).The right panel shows the fluorescence spectra of CaM wild-type (red line), *h*CaM L39C-*mBBr*/V91C-*mBBr* (green line), and inhibitor **TFP** alone (blue line); λ_{ex} = 381 nm, λ_{em} = 400−550 nm.

dx.doi.org/10.1021/jm200167g |*J. Med. Chem.* 2011, 54, 3875–3884

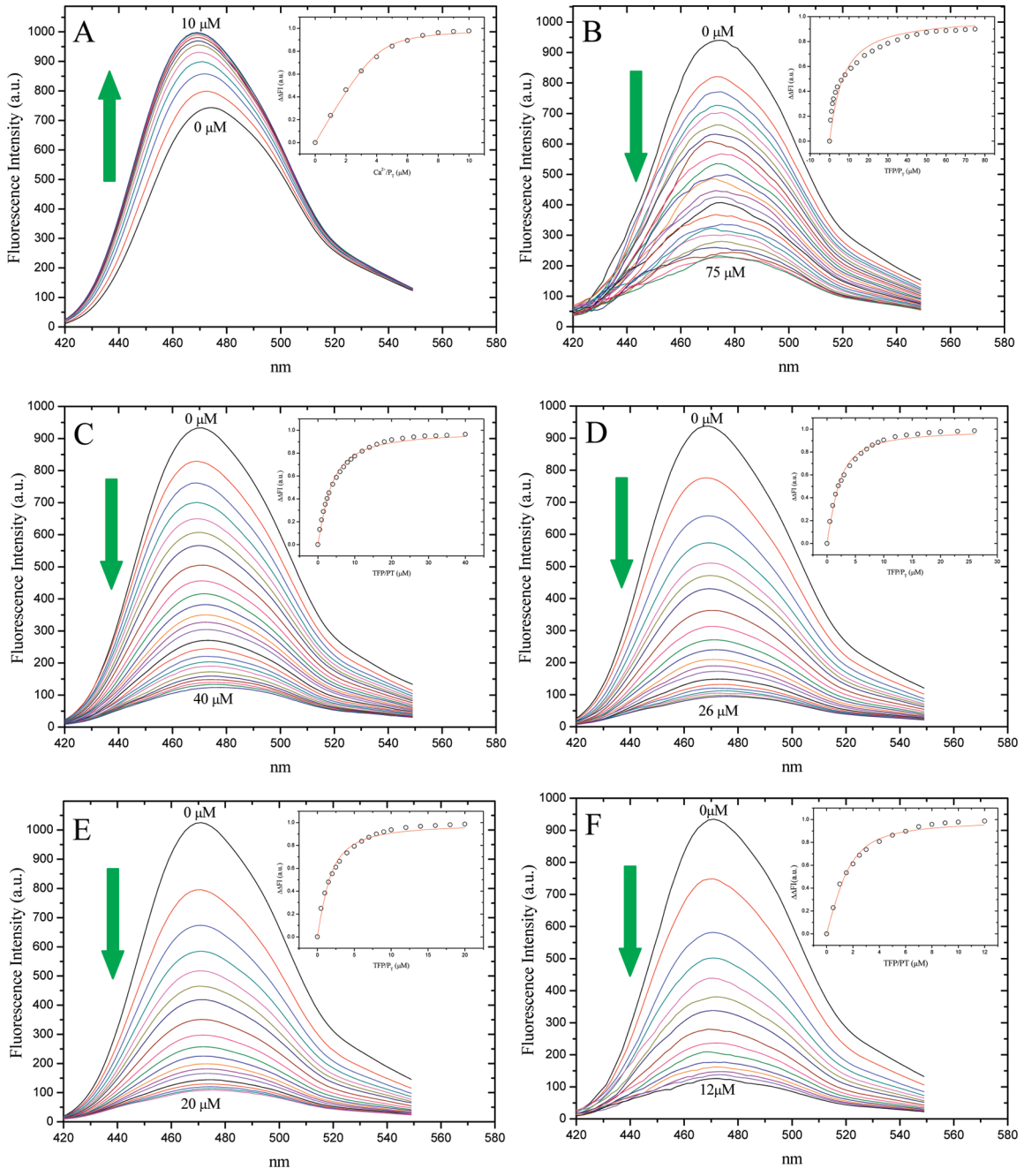

Figure 4. Fluorescence spectra and titration curves of *h*CaM L39C-*mBBr*/V91C-*mBBr* with ion Ca^{2+} (A) and **TFP** (100 μM) at different concentrations of calcium ion: 0.0 μM (B), 2.5 μM (C), 5.0 μM (D), 7.5 μM (E), and 10.0 μM (F). Buffer was 10 mM of potassium acetate (pH 5.1) at 37 °C. Samples were excited at 381 nm, and emission spectra recorded from 415 to 550 nm. The absolute changes of maximal fluorescence emission were corrected for light scattering effects and plotted against the ligands to total protein ratio (insets). The continuous line in the insets comes from the fitting of data to the binding model (eq 1 in Experimental Section) to obtain the K_d and the stoichiometry ratio. The resulting parameter estimates are given in Table 1.

mutagenesis on pET12b-CaM allowed substitution of residues Leu39 and Val91 by Cys (pET13b-CaM L39C/V91C). Then, the resulting plasmid was transformed into *E. coli* BL21-AI One Shot (see, Experimental Section). Altogether, from the biotechnological point of view, the process was efficient and low-cost because the pET12 is one of the most powerful systems developed for cloning and overexpression of recombinant proteins; and on the other hand, the expression induced by L-(+)-arabinose in BL21-AI transformed cells is about 25 times cheaper than IPTG. The overall production of *h*CaM L39C/V91C was optimized successfully to render 30 mg/L of culture medium.

The last step in the biosensor construction was labeling of *h*CaM L39C/V91C with *mBBr* according to the methodology described in the Experimental Section. The incorporation of two fluorophores to the engineered protein (*h*CaM L39C-*mBBr*/V91C-*mBBr*) provides higher quantum efficiency (ϕ = 0.514) in comparison with wild-type *h*CaM (ϕ = 0.025). The improved quantum efficiency directly impacted in the higher sensitivity of this biosensor.

dx.doi.org/10.1021/jm200167g |*J. Med. Chem.* 2011, 54, 3875–3884

Table 1. Binding Properties TFP to the *h*CaM As a Function of the Calcium Concentration

concentration of Ca^{2+} (μM)	K_d (μM)	stoichiometric
0.0	5.7 ± 0.5	2.0 ± 0.2
2.5	2.1 ± 0.1	2.6 ± 0.3
5.0	1.0 ± 0.1	1.8 ± 0.2
7.5	0.8 ± 0.1	1.4 ± 0.2
10.0	0.5 ± 0.07	1.6 ± 0.2

Scheme 1. Chemical Structures of Xanthones Isolated from *Emericella* 25379 [a]

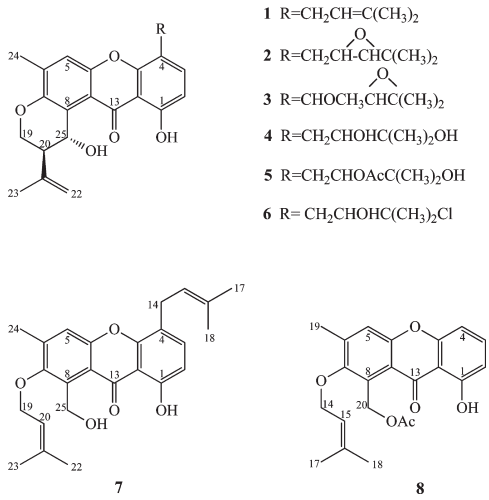

[a] Shamixanthone (**1**), tajixanthone (**2**), 14-methoxytajixanthone (**3**), tajixanthone hydrate (**4**), 15-acetyl tajixanthone hydrate (**5**), 16-chlorotajixanthone (**6**), emericellin (**7**), and variecoxanthone A acetate (**8**).

Properties of the Biosensor (*h*CaM L39C-*mBBr*/V91C-*mBBr*). Figures 3 and 4 show the main spectroscopic properties of the biosensor; the UV λ_{max} values for *h*CaM wild-type (1 μM), *h*CaM L39C-*mBBr*/V91C-*mBBr* (1 μM), and **TFP** (100 μM) were 276, 381, and, 306 nm, respectively. Because of the extrinsic fluorescence of bimane, L39C-*mBBr*/V91C-*mBBr* gives a higher signal-to-noise ratio than the intrinsic UV absorption and fluorescence intensity than *h*CaM wild-type (Figure 3). This biosensor is suitable for monitoring most biological CaM ligands and any chemical compound that does not absorb at 381 nm. As shown in Figure 3, at λ_{ex} 381 nm the fluorescence intensity of **TFP** and *h*CaM wild-type were undetectable while that of *h*CaM L39C-*mBBr*/V91C-*mBBr* was conspicuous.

This biosensor can monitor the binding of CaM to Ca^{2+}, as well as to CaM antagonists by increasing or quenching its fluorescence signal, respectively (Figure 4). Fluorescence titration curves (λ_{ex} 381 nm, λ_{em} 415−550 nm) of *h*CaM L39C-*mBBr*/V91C-*mBBr* were constructed, with Ca^{2+} alone ($CaCl_2$; 0−10 μM) or with **TFP** (0−75 μM) in the absence or presence of different Ca^{2+} concentrations (2.5, 5.0, 7.5 and, 10 μM). The absolute changes of maximal fluorescence emission were plotted against the ratio Ca^{2+}/total protein or **TFP**/total protein and fitted to the binding equation model to obtain the dissociation constants (K_d) values and stoichiometry ratios. For Ca^{2+}, the calculated apparent K_d was 0.24 μM ± 0.03 and the stoichiometry 4.10 ± 0.15; both parameters are in agreement with previously reported data.[15] For **TFP** the apparent K_d was in the range of 5.74−0.53 μM depending on the degree of Ca^{2+} saturation (Table 1). In addition, the system *h*CaM L39C-*mBBr*/V91C-*mBBr* maintained the functional properties of wild type *h*CaM, because it was able to activate PDE1 in vitro (data not show).

In contrast to the previously described *h*CaM M124C-*mBBr*, the new device has the advantage of reporting both Ca^{2+} and *h*CaM ligands with the same system, representing an excellent alternative for the search of new CaM inhibitors, as well as for determining the effects of Ca^{2+} on different CaM ligands (antagonists, proteins or peptides). Then *h*CaM L39C-*mBBr*/V91C-*mBBr*, in contrast to *h*CaM M124C-*mBBr*, could be suitable for detecting classical and nonclassical inhibitors of CaM because the labeled recognition systems are strategically located. Thus, when *h*CaM L39C-*mBBr*/V91C-*mBBr* changes its conformation due to any ligand binding (classical or not classical), quenching of the fluorescence will be always detected. With *h*CaM M124C-*mBBr*, the quenching response will be only observed if classical inhibitors induce the conformational change. The measurements can be performed directly in solution, with high sensitivity and specificity, a very small amount of sample, and it is suitable to quantitative and qualitative determinations.

This development is the subject of the pending patent application No. MX/E/2010/061439, Instituto Mexicano de la Propiedad Industrial (http://www.impi.gob.mx/), 04/10/2010.

Effects of Ca^{2+} on TFP Affinity of CaM. The protein CaM regulates several classes of proteins and enzymes in a Ca^{2+}-dependent manner. Calcium binding to CaM switches its tertiary structure from "semiopen" (Apo-CaM) to "open" ($(Ca^{2+})_4$-CaM complex) stage exposing its hydrophobic patches for binding to specific proteins to induce specific responses.[4,16] It is also known that depiction of hydrophobic areas may change with the degree of Ca^{2+} saturation.[16] In the present work, it has been found that the affinity of **TFP** by *h*CaM is influenced by Ca^{2+} on a concentration-dependent manner; the highest affinity of **TFP** by *h*CaM was observed at a Ca^{2+}:protein ratio of 10:1 while the **TFP**:*h*CaM stoichiometry remained close to 2 (Table 1). This finding reveals the influence of Ca^{2+} concentration on CaM binding parameters with any ligand that binds to *h*CaM in a similar manner as **TFP** and strengthens the relevance of reporting the exact Ca^{2+} concentration employed for K_d calculations of any Ca^{2+}-CaM-ligand complex. For example, in the case of **TFP** different K_d values have been reported, mostly at saturating conditions of Ca^{2+} (the exact concentration is not always indicated), ranging between 1 and 5 μM regardless of the method employed for the calculations.[16] In addition, this allosteric effect of Ca^{2+} on the binding of ligands to CaM might be relevant, and perhaps specific, in some cellular processes regulated by CaM taking place in physiological environments where Ca^{2+} concentration shows significant variation.

Isolation and Characterization of Compounds 1−8. Reinvestigation of the extract from the mycelium and culture medium of the fungus *Emericella* 25379 led to the isolation and characterization of three new analogues of tajixanthone hydrate (**4**),[11] namely 15-acetyl tajixanthone hydrate (**5**), 16-chlorotajixanthone (**6**), and variecoxanthone A acetate (**8**). In addition, the known compounds shamixanthone (**1**), 14-methoxytajixanthone (**3**), tajixanthone (**2**),[17] and emericellin (**7**)[18] were obtained (Scheme 1). The NMR spectra as well as other spectroscopic properties of the known compounds are provided as Supporting Information. The characterization of the new compounds was performed by

Table 2. ^{1}H NMR (500 MHz) and ^{13}C NMR (125 MHz) Data for 15-Acetyl Tajixanthone Hydrate (5), 16-Chlorotajixanthone (6), and Variecoxanthone A Acetate (8) in $CDCl_3$

	5		6		8	
position	δ_C	δ_H, mult (J in Hz)	δ_C	δ_H, mult (J in Hz)	δ_C	δ_H, mult (J in Hz)
1	160.6		160.5		162.0	
2	109.6	6.72 *d* (8.0)	110.3	6.80 *d* (8.0)	110.5	6.78 *dd* (8.0, 1.0)
3	137.8	7.42 *d* (8.0)	137.1	7.52 *d* (8.0)	136.3	7.57 *t* (8.0)
4	109.1		109.3		106.3	6.88 *dd* (8.0, 1.0)
5	119.1	7.33 *q* (1.0)	119.3	7.33 *q* (1.0)	120.9	7.88 *q* (1.0)
6	138.5		138.6		141.6	
7	149.5		149.6		153.8	
8	121.1		119.3		117.7	
9	115.1		115.2		109.3	
10	153.2		152.1		155.5	
11	152.0		152.0		153.9	
12	116.9		121.1		128.4	
13	184.1		184.4		183.0	
14	29.6	a 3.35 *dd* (14.0, 3.0)	28.6	a 3.05 *d* (8.0)	71.8	4.39 *d* (7.5)
		b 2.90 *dd* (14.2, 10.0)		b 3.13 *dd* (16.3, 8.0)		
15	78.6	5.16 *dd* (10.5, 3.0)	63.4	3.03 *dd* (2.0, 10.5)	119.3	5.60 *m*
16	72.4		58.9		139.1	
17	26.9	1.34 *s*	24.8	1.34 *s*	18.0	1.71 *s*
18	25.2	1.38 *s*	19.0	1.46 *s*	25.8	1.83 *s*
19	64.5	a 4.43 *dd* (10.5, 3.2)	64.6	a 4.44 *dd* (10.8, 3.3)	17.5	2.50 *d* (1.0)
		b 4.35 *dd* (11.0, 3.0)		b 4.35 *dd* (11.0, 3.0)		
20	44.9	2.73 *bs*	44.9	2.74 *dd* (3.0, 3.5)	58.0	5.79 *s*
21	142.6		142.6			
22	112.2	a 4.80 *s*	112.3	a 4.82 *dd* (2.5, 1.5)		
		b 4.57 *s*		b 4.60 *dd* (2.5, 1.5)		
23	22.5	1.85 *s*	22.5	1.87 *s*		
24	17.4	2.36 *d* (1.0)	17.4	2.37 *d* (1.0)		
25	63.1	5.41 *s*	63.2	5.43 *ddd* (3.5, 3.0, 1.0)		
CH_3COO	20.7	1.87 *s*			20.9	2.10 *s*
CH_3COO	170.2				170.9	
OH-1		12.56 *s*		12.66 *s*		12.90 *s*
OH-15				2.47 *s*		
OH-16		2.37 *s*				
OH-25		4.96 *d* (4.0)		4.94 *bs*		

conventional spectroscopic and spectrometric techniques (Tables 2, and Supporting Information Figures S10−S13, S15, and S16). The spectroscopic data confirmed the structural relationship of compounds **5**, **6**, and **8** to tajixanthone hydrate (**4**).[11] Thus, the NMR data of **5** (Table 2) clearly revealed the presence of an acetoxy attached to C-15 instead of a hydroxyl group as in the case of **4**. Chemical transformation of compound **5** into **4**, through a hydrolysis reaction under basic conditions, provides additional evidence of the structure of **5** including the absolute configuration at its stereogenic centers. On the other hand, the isotopic pattern in the mass spectrum of **6**, with a typical M/M + 2 ratio of approximately 100:35, revealed the presence of one chlorine atom in the molecule. The ^{1}H and ^{13}C NMR (Table 2) and were almost identical to those of compound **4**, differing only in the chemical shifts of the signal of C-16, which was diamagnetically shifted, suggesting that the hydroxyl group at C-16 in **4** was replaced by a chlorine atom in **6**. Biogenetic considerations strongly supported that the absolute configuration at the stereogenic centers of **6** was the same as that for compounds **4** and **5**. Finally, compound **8** was very similar to emericellin (**7**) except for the absence of the isoprenyl chain at C-4, which was consistent with the typical ABC spin system observed for H-2-H-4 in the ^{1}H NMR of **8**, and the presence of an acetoxy group attached to the methylene group at C-20 as revealed by the paramagnetic shift of the corresponding signals and the presence of resonances for an acetic acid residue (Table 2).

Binding Properties of Xanthones 1−8 on *h*CaM Biosensor. The affinity of xanthones **1**−**8** with $(Ca^{2+})_4$-*h*CaM in solution was measured using the fluorescent biosensor (*h*CaM L39C-*mBBr*/V91C-*mBBr*). The results showed that all compounds but **6** bind to the protein with K_d values in the nM range (Table 3, Figure 5 and Supporting Information Figures S17−S24). Xanthones **2**, **7**, and **1** showed the best affinity to $(Ca^{2+})_4$-*h*CaM complex (K_d = 3.7, 6.8, and 28.7 nM, respectively). These affinities are

dx.doi.org/10.1021/jm200167g |*J. Med. Chem.* 2011, 54, 3875–3884

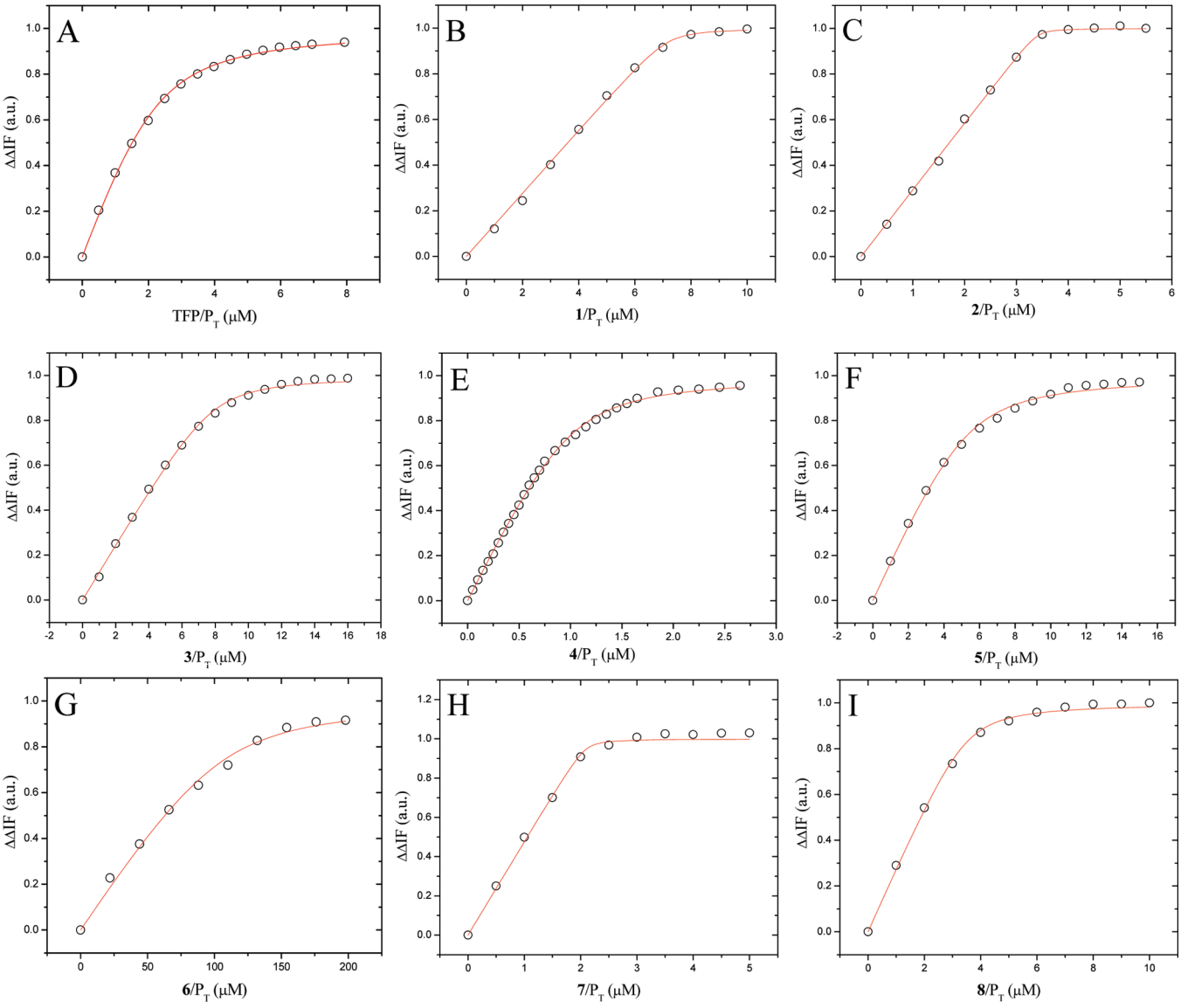

Figure 5. Titration curves of *h*CaM L39C-*mBBr*/V91C-*mBBr* with (A) **TFP**, (B) shamixanthone, (C) tajixanthone, (D)14-methoxytajixanthone, (E) tajixanthone hydrate, (F) 15-acetyl tajixanthone hydrate, (G)16-chlorotajixanthone, (H) emericellin, and (I) variecoxanthone A acetate at saturation concentration of calcium ion. The absolute changes of maximal fluorescence emission were plotted against the ratio ligands/protein total and fitted to the binding model (see eq 1 in Experimental Section) to obtain the K_d and stoichiometric ration.

relevant because most CaM antagonists shown K_d values in the μM order; for example, the phenothiazine derivatives chlorpromazine (CPZ) and **TFP** showed K_d from 1 to 5 μM,[19,20] and the bis-indol alkaloids vinblastine and KAR-2 exhibited K_d of 3.0 and 5.2 μM, respectively.[21] Only the target peptide M13 (1−100 nM)[22] and compound AAA (18 nM)[23] have previously shown K_d values in the nM range. In agreement with previously reported stoichiometry binding data for most CaM-ligands,[24−26] the stoichiometry ratio for xanthones **1**−**8**:CaM ranged from 1 to 10.

According to the data summarized in Table 3, small structural differences of these ligands greatly affect the affinity of the $(Ca^{2+})_4$-*h*CaM complex. Thus, contrasting the K_d values of compounds **7** (6.8 nM), and **8** (124.7 nM) as well as those of **1** (28.7 nM) and **7**, revealed that the presence of an isoprenyl chain at C-4 and opening of the pyran ring, respectively, increased the affinity for the protein. On the other hand, comparison of K_d values of **2** (3.7 nM), **3** (235.1 nM), and **4** (93.0 nm) indicated that the presence of any substituent at C-14 as in compound **3** or the opening of the epoxy functionally of compound **2** decreased the affinity by $(Ca^{2+})_4$-*h*CaM complex. Finally, replacement of the OH at C-16 (as in **4**) for a chlorine group, as in **6** (K_d = 7.3 μM), increased the affinity toward $(Ca^{2+})_4$-*h*CaM complex.

In summary, the xanthones **1**−**8** from *Emericella* 25379 are flexible molecules, possessing a hydrophobic region and a partially negative charged side chain. These structural characteristics correlate with good CaM binding affinity, because this protein is rich in negatively charged amino acid and methionine residues which can interact with partially charged and hydrophobic ligand, respectively. Altogether, these interactions may contribute to the stabilization of the $(Ca^{2+})_4$-*h*CaM-ligand complexes and impair the physiological functions of CaM.

Docking Studies. With the aim to obtain a binding model of compounds **1**−**8** with CaM (PDB code 1LIN), a molecular docking study was performed using the program AUTODOCK

dx.doi.org/10.1021/jm200167g |*J. Med. Chem.* 2011, 54, 3875–3884

Table 3. Binding and Docking Properties of Compounds 1−8 to Ca^{2+}-CaM Complex

	fluorescence quenching		docking	
compd	K_d (nM)	stoichiometric	K_i (nM)	site[b]
TFP	532.7 ± 74.2	1.6 ± 0.2	24.2	1
1	28.8 ± 1.4	7.1 ± 0.1	83.0	1
2	3.7 ± 0.2	3.4 ± 0.2	53.4	1
3	23.1 ± 41.4	7.8 ± 1.3	26.9	1
4	93.0 ± 4.3	1.1 ± 0.01	8.6	1
5	498.4 ± 52.3	5.3 ± 0.2	3.1	1
6	7.3 ± 2.6[a]	ND[c]	76.9	4
7	6.8 ± 0.07	2.0 ± 0.06	137.3	3
8	124.7 ± 22.1	3.5 ± 0.11	282.1	1

[a] The concentration is μM. [b] Number of site of binding to CaM (see, text). [c] ND, not determined.

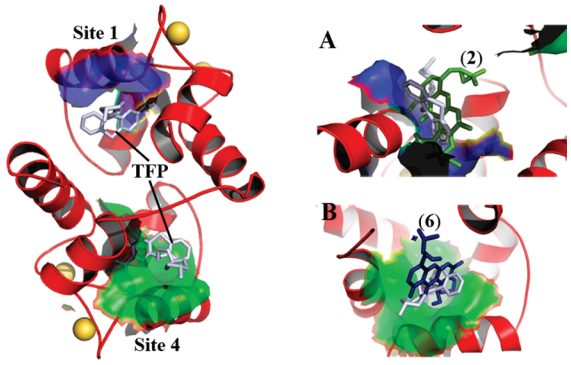

Figure 6. Structural model of Ca^{2+}-CaM-**TFP** complex represented in red cartoon and surface showing the pocket of binding to **TFP** corresponding to sites 1 and 4. The amino acids comprising site 1 are Phe92, Ile100, Leu105, Met124, Ile125, Glu127, Ala128, Val136, Phe141, and Met144 (surface blue) and those in site 4 are Phe19, Ile27, Leu32, Met51, Ile52, Glu54, Val55, Ile63, Phe68, and Met71 (surface green). The left panel shows the binding of **TFP** (white sticks) to sites 1 and 4, taken from the crystallographic structure of the Ca^{2+}-CaM-**TFP** complex (pdb 1LIN). The right panel shows the binding models of compounds **2** and **6** with the Ca^{2+}-CaM complex. CaM is represented in red cartoon, **TFP** is depicted in white sticks, **2** (tajixanthone) in lime sticks, and **6** (16-chlorotajixanthone) in blue sticks. This figure was prepared using PyMOL.[32]

4.0.2.[27,28] First, all ligand structures were optimized with the program Gaussian 09 using the density functional theory method (DFT) at the B3LYP/3-21G level. Then, the ligands were docked into the entire protein. The best conformations observed in this preliminary analysis were docked into a smaller area (grid) in order to refine the results. All compounds analyzed bound to the pocket corresponding to site I except compound **6** and **7**, which bind to sites IV and III, respectively (Figure 6 and Supporting Information Figure S29). These binding sites have been identified as the most common binding regions for most CaM-ligands, including **TFP**.[29] Subtle structural differences might account for these differences. Figure 6 shows the theoretical binding model for **2** and **6** superimposed with the X-ray structure of the protein with the classical inhibitor **TFP**. Supporting Information Figures S25−S30 show the dockings for **1**, **3**−**5**, **7**, and **8**. The excellent affinity of these compounds may be due to their ability to bind $(Ca^{2+})_4$-CaM throughout lipophilic and polar protein−ligand contact surface interactions.

CONCLUSIONS

A new highly specific fluorescent biosensor of *h*CaM (*h*CaM L39C-*mBBr*/V91C-*mBBr*), capable of detecting both anti-CaM compound and calcium ions with excellent sensitivity has been developed. The biosensor was stable under normal storage conditions and showed good stability over a large number of assays. Using this new tool, we studied the allosteric effect of Ca^{2+} on **TFP** binding to *h*CaM. This effect could be important at the physiological level because CaM relies in different modes of Ca^{2+}-dependent protein−protein interactions to control a wide range of metabolic processes. Those binding modes are responsible for the CaM high affinity and specificity for its many molecular targets. In turn, such finely tuned changes in affinity and specificity are required to explain the subtle modulation of simultaneous Ca^{2+}-CaM mediated cellular responses.

The binding properties of eight xanthones on $(Ca^{2+})_4$-*h*CaM complex were assessed using this biosensor. The results revealed affinities in the nM range. Docking analyses were consistent with these results and predicted that these natural products bind to pockets I, III, and IV, where the classical inhibitor **TFP** binds.

EXPERIMENTAL SECTION

CALM1 (human phosphorylase kinase, δ) gene was purchased from Origene Technology (Rockville, MD). pGEM-T Easy Vector System I was purchased from Promega (Madison, WI). pET12b vector was obtained from Novagen (Darmstadt, Germany). *Pfu* DNA polymerase was purchased from Stratagene (La Jolla, CA). *NdeI* and *Bam*HI were obtained from New England Biolabs (Ipswich, MA). Primers for polymerase chain reaction (PCR) mutagenesis and *Escherichia coli* BL21-AI One Shot were purchased from Invitrogen (Carlsbad, CA). Monobromobimane (*mBBr*) was purchased from Toronto Chemical Research (Toronto). All other reagents were of analytical reagent grade and were purchased from Sigma (St. Louis, MO).

Subclonig of Gene Encoding for *h*CaM and Site-Directed Mutagenesis. *CALM1* gene encoding *h*CaM was amplified using PCR from the cDNA (cDNA) clone pCMV6-XL5 (Origene Technology) along with the primers (5′-CATATGGCTGATCAGCTGACCG-3′ and 5′-CCTAGGAGTAAAACGTCAGTAGT AGAC-3′) to insert restriction sites *NdeI* and *Bam*HI at the start and end of the gene. Amplified products were cloned into a vector (pGEM-T Easy Vector System I) and further subcloned into the expression vector pET12b from the Novagen (EMD Chemicals, Darmstadt, Germany). Amino acid substitutions were generated by overlapping PCR mutagenesis using the Quick Change Kit (Stratagene, La Jolla, CA). The amount of plasmid (containing the gene encoding *h*CaM) pET12b-*h*CaM was 100 ng, and the amount of mutagenic oligonucleotides was 125 ng. PCR amplification included 25 cycles of denaturation at 95 °C for 1 min, annealing using a temperature ramp from 45 to 60 °C a heating rate of 0.2 °C/s and polymerization at 68 °C for 10 min, followed by one final extension step at 68 °C for 10 min. Oligonucleotides used to generate the single mutant L39C were 5′-CATGAGGTCATGTGGTCAGAACCC-3′ and 5′-GGGTTCTGACCACATGACCTCATG-3′; for the double mutant L39C/V91C, 5′-GGCATTCCGATGCTTTGACAAGG-3′ and 5′-CCTTGTCAAAGCATCGGAATGCC-3′. After the mutagenesis experiments, the products of PCR amplification were digested with *DpnI* enzyme and transformed in DH5α competent cells. The sequences of all constructs and mutations were confirmed by nucleotide sequencing with an ABI PRISM 310 genetic analyzer (Applied Biosystems, Foster City, CA).

Plasmids (pET12b-*h*CaM L39C/V91C) were transformed into *E. coli* BL21-AI One Shot following the specifications of the kit's manufacturer.

Protein Purification of *h*CaM L39C/V91C. A single colony of *E. coli* strain BL21-AI/pET12b-*h*CaM L39C/V91C was grown in Luria−Bertani (LB) medium containing 100 mg/mL of ampicillin overnight with shaking at 37 °C and was inoculated into 500 mL of LB medium containing 100 mg/mL of ampicillin until the optical density (OD) of the culture at 550 nm reached between 0.8 and 1.0. Expression was induced by the addition of L-(+)-arabinose (0.2%, w/v) overnight with shaking at 37 °C. The cells were harvested by centrifugation (10 min, 4000*g*), suspended in 50 mM Tris-HCl, 2 mM ethylenediaminetetraacetic acid (EDTA), 1 mM dithiothreitol (DTT), and 200 mg/mL of egg white lysozyme at pH 7.5 and were chilled on ice for 30 min. Suspended cells were lysed by sonication, and cellular debris was removed by centrifugation for 15 min at 15000*g*. The supernatant was collected, and $CaCl_2$ and NaCl were added to final concentrations of 5 and 500 mM, respectively. The protein was purified using a Phenyl Sepharose CL-4B chromatographic column. Briefly, the supernatant was applied to the column pre-equilibrated with 50 mM Tris-HCl, 0.5 mM DTT, 0.1 mM $CaCl_2$, and 500 mM NaCl at pH 7.5. The column was washed with loading buffer, followed by the same with 1 mM EDTA and 150 mM NaCl. Finally, the protein was loaded on a cationic exchange column (Source Q, Amersham Biosciences, Piscataway, NJ) at pH 8.8 and was eluted by a linear gradient of 40 min (0−100%) with 500 mM NaCl. Protein was collected in fractions and assessed for purity by gel electrophoresis. All preparations were at least 98% pure by this criterion.

Chemical Modification of Unique Reactive Cysteine of *h*CaM L39C/V91C Protein with *mBBr*. All fluorophore conjugations steps were typically carried out at room temperature. To a protein at a concentration of 5−10 mg/mL, 5 mM of DTT was added and incubated for 3 h to reduce intramolecular disulfide bonds, and then it was washed on a gel filtration HR-100 column (Pharmacia Biotech, Piscataway, NJ). A thiol-reactive fluorophore (20% in DMSO) was added in small aliquots to reach a final concentration of 10 molar and DMSO of approximately 5%. Conjugation proceeded in the dark overnight at 4 °C. Separation of protein from unreacted fluorophore was achieved by size exclusion chromatography with a Superdex 75 column (Pharmacia Biotech, Piscataway, NJ). The efficiency of report group attachment was assessed by reactivity of the protein against 5-5′-dithiobis-(2-nitrobenzoic) acid (DTNB), measuring the release of 2-nitrobenzoate (TNB). Next, protein concentrations of *h*CaM L39C-*mBBr*/V91C-*mBBr* were determined with the bicinchoninic acid method.[30]

Steady-State Fluorescence. All measurements were conducted with an ISS-PC1 spectrofluorometer (ISS, Champaign, IL) with sample stirring at 37 °C. The protein *h*CaM L39C-*mBBr*/V91C-*mBBr* (1 μM) was incubated in buffer (10 mM of potassium acetate [pH 5.1] and $CaCl_2$ to saturation). Fluorescence emission spectra were acquired with excitation and emission slit widths of 4 and 8 nm, respectively. The excitation wavelength was 381 nm, and emission wavelengths of 415−550 nm were measured. The fractional degree of saturated *h*CaM L39C-*mBBr*/V91C-*mBBr* with ligand (y) was calculated by changes in fluorescence on ligand binding according to $y = (F - F_0)/(F_\infty - F_0)$, where F_∞ represents the fluorescence intensity at saturation of the ligand, y is plotted as a function of the protein/ligand relation (L), and the apparent dissociation constants (K_d) and stoichiometric (S) were obtained by fitting to the equation:

$$y = \left((1 + K_d/S + L/S) - \sqrt{(1 + K_d/S + L/S)^2 - 4L/S}\right)/2$$

where y represents the fractional degree of fluorescence intensity at 470 nm, K_d is the apparent dissociation constant for the ligands, L is the protein/ligand relation, and S is the stoichiometric. The data were analyzed using the Origin version 8.0 program (OriginLab, Northampton, MA).

Before testing all compounds were purified by HPLC using the condition indicated in the extraction and isolation section.

Molecular Modeling. Docking was conducted using the PDB X-ray structure of CaM with TFP (1LIN.pdb). The crystal structure was rebuilt and refined after several iterations; final all-atom refinement of CaM was carried out with Rosetta 3.1.[31] All compounds were built using the program HyperChem 8 and optimized geometrically using the program Gaussian 09, revision A.02 (Gaussian Inc., Wallingford, CT) at DTF B3LYP/3-21G level of theory. The protein and ligands were further prepared using the utilities implemented by AutoDockTools 1.5.4 (http://mgltools.scripps.edu/). The protein was adding polar hydrogen atoms, Kollman united-atom partial charges and to the ligands computing Gasteiger−Marsilli formalism charges, rotatable groups which were assigned automatically as were the active torsions. Blind docking was carried out using AutoDock4 version 4.2 software (http://autodock.scripps.edu/)[27,28] using the default parameters the Lamarkian genetic algorithm with local search, number of individuals in population (150), maximum number of energy evaluations (2.5 million), maximum number of generations (27000), rate of gene mutation (0.02), rate of crossover (0.8), and 100 runs for docking. Electrostatic grid maps were generated for each atom type in the ligands using the auxiliary program AutoGrid4 part of the software AutoDock4. The initial grid box size was 60 Å × 60 Å × 60 Å in the x, y, and z dimensions. In order a refined docking analysis was performed in a smaller grid box, with 30 Å × 30 Å × 30 Å dimensions, placed in the ligand. All calculations were made using a parallel distributed memory supercomputer (Kanbalam, Dirección General de Cómputo y de Tecnologías de Información y Comunicación, UNAM) which contains 1368 processors AMD Opteron, around 3 terabyte of memory, and 160 terabyte of storage (http://www.super.unam.mx/). The analysis of the docking was made with AutoDockTools using cluster analysis and program PyMOL.[32]

Collection of Physical and Spectroscopic Parameters of Xanthones 1−8. Melting points were determined in a Fisher−Johns apparatus and are uncorrected. The IR spectra were obtained using KBr, film or reflectance on a Perkin-Elmer 599B spectrophotometer. UV spectra were recorded in a Shimadzu 160 UV spectrophotometer at 25 °C in $CHCl_3$ solution. ^{1}H, ^{13}C, and 2D NMR were recorded on a Varian Unity Plus 300 or a Bruker spectrometers at 300 MHz (^{1}H)/100 MHz (^{13}C) and 500 MHz (^{1}H)/125 MHz (^{13}C), respectively, in $CDCl_3$ or CD_2Cl_2 using tetramethylsilane (TMS) as an internal standard; chemical shifts were recorded as δ values. EIMS was measured in a JEOL JMS AX-505HA mass spectrophotometer.

Fungal Material. The fungus *Emericella* 25379 was isolated from the surface of a coral (*Pacifigorgia rutilia*), collected at Marietas Islands, Nayarit, Mexico, in 2006. Cultures of the fungus are maintained in a mycological collection of the Laboratorio de Micopatología, Instituto de Biología, UNAM. Stock cultures of the fungus were stored at 4 °C on agar plates of potato dextrose agar (PDA). In addition subcultures were obtained in V8 and PDA medium.

Fermentation. Two flask, each containing the liquid medium (10 L/flask) composed of Czapek concentrate (10 mL/L), K_2HPO_4 (1 g/L), powdered yeast extract (5 g/L), and sucrose (30 g/L) were individually inoculated with 1 cm^2 agar plug taken from a stock culture. Flasks were cultured for 30 days at room temperature in static conditions. After the fermentation, all broth (20 L) was filtrated to give supernatant and mycelia. Next, the filtered growth medium was exhaustively extracted with CH_2Cl_2, and the resultant solution was concentrated in vacuo. The mycelium was macerated with CH_2Cl_2 (3 × 2 L). The organic solution was dried on anhydrous sodium sulfate (Na_2SO_4), and subsequently concentrated under reduced pressure. The organic extracts obtained from mycelia and culture medium were combined based on the chromatographic profiles to give a dark brown solid (5.0 g).

Extraction and Isolation. Open column chromatography was performed on Silica Gel 60 (0.063−0.200 mm), 70−230 Mesh (Merck, Darmstadt), or Sephadex LH-20. Preparative thin layer chromatography (TLC) was carried out on Silica Gel PF_{254}. Preparative HPLC was

performed using a SymmetryPrep C_{18} column 7 μm (Waters) [7.8 mm × 300 mm, 2.4 mL/min]. Control of the equipment, data acquisition, processing, and management of chromatographic conditions were performed by the Empower 2 software program (Waters).

The organic extract (5.0 g), was initially fractionated by Silica Gel column chromatography, eluting with gradient systems of hexane-CH_2Cl_2-MeOH. Each fraction (100 mL) was monitored by TLC, and fractions with similar patterns were combined to yield eleven primary fractions ($\mathbf{F_1}$−$\mathbf{F_{11}}$). Fraction $\mathbf{F_4}$ (50 mg) was subjected to preparative TLC (hexane-EtOAc 7:3) to yield shamixanthone **1** (9.1 mg) and emericellin **7** (20 mg). The resolution of $\mathbf{F_5}$ (212 mg) by open column chromatography on Sephadex LH-20 led to five subfractions, designed as, $\mathbf{F_{5-I}}$−$\mathbf{F_{5-V}}$. $\mathbf{F_{5\text{-}V}}$ (30 mg) was resolved by reverse phase HPLC, eluting with ACN to yield variecoxanthone A acetate **8** (6.0 mg). The analysis of $\mathbf{F_7}$ (54 mg) by HPLC, using the same conditions, led to the isolation of tajixanthone **2** (12.0 mg) and 14-methoxytajixanthone **3** (15 mg). Fraction $\mathbf{F_9}$ (150 mg) was chromatographed on Sephadex LH-20, eluted with MeOH to give six subfractions $\mathbf{F_{9-I}}$−$\mathbf{F_{9-VI}}$. Purification of $\mathbf{F_{9-III}}$ (35 mg) by open CC on Sephadex LH-20, eluting with CH_2Cl_2, gave 15-acetyl tajixanthone hydrate **5** (3.0 mg). Subfraction $\mathbf{F_{9-II}}$ (40 mg) was further purified by preparative TLC (CH_2Cl_2−MeOH 99:1) to yield 16-chlorotajixanthone **6** (4.0 mg). Finally purification of fraction $\mathbf{F_{10}}$ (45 mg) on a reverse phase HPLC gave tajixanthone hydrate **4** as a yellow solid (15.0 mg).

Basic Hydrolysis of Compound 5. First, 4 mg of ester **5** in MeOH (1 mL) were placed in a 25 mL round-bottomed flask mounted over a magnetic stirrer and maintained at 35 °C. Then methanolic KOH (10%) solution (1 mL) was added and the contents were stirred. The reaction was quenched after 60 min by addition of 3 mL of H_2O. The mixture was neutralized with 1 N hydrochloric acid and extracted with $CHCl_3$ (3 mL × 3). The combined organic extracts were dried with Na_2SO_4 and concentrated in vacuo to yield compound **4**.

*15-Acetyl Tajixanthone Hydrate (**5**).* Yellow needles, mp 206−208 °C. IR υ_{max} (KBr)/cm^{-1} 3421, 2925, 1734, 1742, 1602, 1575, 1475, 1243, 989, 896, 823. UV λ_{max} ($CHCl_3$)/nm (log ε) 388 (3.60), 339 (3.25), 301 (3.76), 292 (3.72), 277 (4.07), 258 (3.96), 249 (3.92), 244 (3.94). HRMS-EI $[M]^+$ m/z 482.522 (calcd for $C_{27}H_{30}O_8$ 482.530).

*16-Chlorotajixanthone (**6**).* Yellow needles, mp 179−180 °C. IR υ_{max} (KBr)/cm^{-1} 3486, 3073, 2925, 2849, 1736, 1644, 1567, 1240, 1022, 920. UV λ_{max} ($CHCl_3$)/nm (log ε) 388 (3.60), 339 (3.25), 301 (3.76), 292 (3.72), 277 (4.07), 258 (3.96), 249 (3.92), 244 (3.94). HRMS-EI $[M]^+$ m/z 458.150 (calcd for $C_{25}H_{27}O_6Cl$ 458.149).

*Variecoxanthone A Acetate (**8**).* Yellow needles, mp 89−90 °C. IR υ_{max} (reflectance)/cm^{-1} 3482, 2926, 2855, 1736, 1644, 1601, 1467, 1232. UV λ_{max} ($CHCl_3$)/nm (log ε) 234 (0.64), 258 (0.64), 287 (0.26), 370 (0.14). HRMS-FAB $[M + 1]^+$ m/z 383.411 (calcd for $C_{22}H_{22}O_6$ 383.406).

■ ASSOCIATED CONTENT

Supporting Information. Physical and spectroscopic parameters of xanthones **1**, **3**−**5**, **7**, and, **8**. Fluorescence spectra changes of the titration of *h*CaM L39C-*mBBr*/V91C-*mBBr* with compound **1**−**8** and structural models of Ca^{2+}-CaM with **1**, **3**−**5**, **7**, and **8**. This material is available free of charge via the Internet at http://pubs.acs.org.

■ AUTHOR INFORMATION

Corresponding Author

*Phone: +525 55 622 5289. Fax: +525 55 622 5329. E-mail: rachel@servidor.unam.mx.

■ ACKNOWLEDGMENT

This work was supported by grants from DGAPA-UNAM (IN218110) and CONACyT 99395. We thank Georgina Duarte, Margarita Guzmán, Nuria Esturau, Marisela Gutierrez, Isabel Rivero, and Araceli Pérez for their valuable technical assistance. The authors are very grateful to Dr. A. Olson and his colleagues at the Scripps Research Institute for providing AutoDock. José Rivera-Chávez acknowledges a fellowship from CONACyT. Martin González-Andrade acknowledges postdoctoral fellowship, awarded by DGAPA-UNAM. We are indebted to Dirección General de Cómputo y de Tecnologías de Información y Comunicación, UNAM, for providing the resources to carry out the computational calculations through the KanBalam supercomputing cluster.

■ ABBREVIATIONS USED

*h*CaM, human calmodulin; CaM, protein calmodulin; PDE1, calmodulin-sensitive *c*AMP phosphodiesterase; C*ALM1*, gene human phosphorylase kinase δ; TFP, trifluoroperazine; CPZ, chlorpromazine; *mBBr*, monobromobimane; Ca^{2+}, calcium; EDTA, ethylenediaminetetraacetic acid; DTT, dithiothreitol; DMSO, dimethyl sulfoxide; ACN, acetonitrile; DTNB, 5-5′-dithiobis-(2-nitrobenzoic) acid; TNB, 2-nitrobenzoate; TMS, tetramethylsilane; PDA, potato dextrose agar; K_d, dissociation constants; NMR, nuclear magnetic resonance; PDB, protein data bank; DFT, density functional theory; EFEB, estimated free energy of binding; PCR, polymerase chain reaction; TLC, thin layer chromatography; HPLC, high performance liquid chromatography

■ REFERENCES

(1) Keusgen, M. Biosensors: new approaches in drug discovery. *Naturwissenschaften* **2002**, *89*, 433–444.

(2) Geiser, J. R.; van Tuinen, D.; Brockerhoff, S. E.; Neff, M. M.; Davis, T. N. Can calmodulin function without binding calcium? *Cell* **1991**, *65*, 949–959.

(3) Bouche, N.; Yellin, A.; Snedden, W. A.; Fromm, H. Plant-specific calmodulin-binding proteins. *Annu. Rev. Plant. Biol.* **2005**, *56*, 435–466.

(4) Chin, D.; Means, A. R. Calmodulin: a prototypical calcium sensor. *Trends Cell Biol.* **2000**, *10*, 322–328.

(5) Seales, E. C.; Micoli, K. J.; McDonald, J. M. Calmodulin is a critical regulator of osteoclastic differentiation, function, and survival. *J. Cell Biochem.* **2006**, *97*, 45–55.

(6) Du, J.; Szabo, S. T.; Gray, N. A.; Manji, H. K. Focus on CaMKII: a molecular switch in the pathophysiology and treatment of mood and anxiety disorders. *Int. J. Neuropsychopharmacol.* **2004**, *7*, 243–248.

(7) Sharma, R. K.; Das, S. B.; Lakshmikuttyamma, A.; Selvakumar, P.; Shrivastav, A. Regulation of calmodulin-stimulated cyclic nucleotide phosphodiesterase (PDE1): review. *Int. J. Mol. Med.* **2006**, *18*, 95–105.

(8) Nijjar, M. S.; Nijjar, S. S. Domoic acid-induced neurodegeneration resulting in memory loss is mediated by Ca^{2+} overload and inhibition of Ca^{2++} calmodulin-stimulated adenylate cyclase in rat brain (review). *Int. J. Mol. Med.* **2000**, *6*, 377–389.

(9) Dikici, E.; Deo, S. K.; Daunert, S. A whole-cell assay for the high throughput screening of calmodulin antagonists. *Anal. Bioanal.Chem.* **2008**, *390*, 2073–2079.

(10) Gonzalez-Andrade, M.; Figueroa, M.; Rodriguez-Sotres, R.; Mata, R.; Sosa-Peinado, A. An alternative assay to discover potential calmodulin inhibitors using a human fluorophore-labeled CaM protein. *Anal. Biochem.* **2009**, *387*, 64–70.

(11) Figueroa, M.; Gonzalez M del, C.; Rodriguez-Sotres, R.; Sosa-Peinado, A.; Gonzalez-Andrade, M.; Cerda-Garcia-Rojas, C. M.; Mata, R. Calmodulin inhibitors from the fungus *Emericella* sp. *Bioorg. Med. Chem.* **2009**, *17*, 2167–2174.

(12) Pouli, N.; Marakos, P. Fused xanthone derivatives as antiproliferative agents. *Anticancer Agents Med. Chem.* **2009**, *9*, 77–98.
(13) Na, Y. Recent cancer drug development with xanthone structures. *J. Pharm. Pharmacol.* **2009**, *61*, 707–712.
(14) Mansoor, S. E.; McHaourab, H. S.; Farrens, D. L. Determination of protein secondary structure and solvent accessibility using site-directed fluorescence labeling. Studies of T4 lysozyme using the fluorescent probe monobromobimane. *Biochemistry* **1999**, *38*, 16383–16393.
(15) Linse, S.; Helmersson, A.; Forsen, S. Calcium binding to calmodulin and its globular domains. *J. Biol. Chem.* **1991**, *266*, 8050–8054.
(16) Feldkamp, M. D.; O'Donnell, S. E.; Yu, L.; Shea, M. A. Allosteric effects of the antipsychotic drug trifluoperazine on the energetics of calcium binding by calmodulin. *Proteins* **2010**, *78*, 2265–2282.
(17) Chexal, K. K.; Fouweath., C; Holker, J. S. E.; Simpson, T. J.; Young, K. Biosynthesis of Fungal Metabolites 0.3. Structure of Shamixanthone and Tajixanthone, Metabolites of *Aspergillus variecolor*. *J. Chem. Soc., Perkin Trans. 1* **1974**, 1584–1593.
(18) Kawahara, N.; Nakajima, S.; Yamazaki, M.; Kawai, K. Structure of a novel epidithiodioxopiperazine, emethallicin A, a potent inhibitor of histamine release from *Emericella heterothallica*. *Chem. Pharm. Bull. (Tokyo)* **1989**, *37*, 2592–2595.
(19) Johnson, J. D.; Wittenauer, L. A. A fluorescent calmodulin that reports the binding of hydrophobic inhibitory ligands. *Biochem. J.* **1983**, *211*, 473–479.
(20) Figueroa, M.; González-Andrade, M.; Sosa-Peinado, A.; Madariaga-Mazón, A.; Del Río-Portilla, F.; Del Carmen González, M.; Mata, R. Fluorescence, circular dichroism, NMR, and docking studies of the interaction of the alkaloid malbrancheamide with calmodulin. *J. Enzyme Inhib. Med. Chem.* **2010**, 1–8.
(21) Vertessy, B. G.; Harmat, V.; Bocskei, Z.; Naray-Szabo, G.; Orosz, F.; Ovadi, J. Simultaneous binding of drugs with different chemical structures to Ca^{2+}-calmodulin: crystallographic and spectroscopic studies. *Biochemistry* **1998**, *37*, 15300–15310.
(22) Green, D. F.; Dennis, A. T.; Fam, P. S.; Tidor, B.; Jasanoff, A. Rational design of new binding specificity by simultaneous mutagenesis of calmodulin and a target peptide. *Biochemistry* **2006**, *45*, 12547–12559.
(23) Harmat, V.; Bocskei, Z.; Naray-Szabo, G.; Bata, I.; Csutor, A. S.; Hermecz, I.; Aranyi, P.; Szabo, B.; Liliom, K.; Vertessy, B. G.; Ovadi, J. A new potent calmodulin antagonist with arylalkylamine structure: crystallographic, spectroscopic and functional studies. *J. Mol. Biol.* **2000**, *297*, 747–755.
(24) Levin, R. M.; Weiss, B. Binding of trifluoperazine to the calcium-dependent activator of cyclic nucleotide phosphodiesterase. *Mol. Pharmacol.* **1977**, *13*, 690–697.
(25) Massom, L.; Lee, H.; Jarrett, H. W. Trifluoperazine binding to porcine brain calmodulin and skeletal muscle troponin C. *Biochemistry* **1990**, *29*, 671–681.
(26) Rao, S. T.; Wu, S.; Satyshur, K. A.; Ling, K. Y.; Kung, C.; Sundaralingam, M. Structure of *Paramecium tetraurelia* calmodulin at 1.8 A resolution. *Protein Sci.* **1993**, *2*, 436–447.
(27) Morris, G. M.; Goodsell, D. S.; Halliday, R. S.; Huey, R.; Hart, W. E.; Belew, R. K.; Olson, A. J. Automated docking using a Lamarckian genetic algorithm and an empirical binding free energy function. *J. Comput. Chem.* **1998**, *19*, 1639–1662.
(28) Huey, R.; Morris, G. M.; Olson, A. J.; Goodsell, D. S. A semiempirical free energy force field with charge-based desolvation. *J. Comput. Chem.* **2007**, *28*, 1145–1152.
(29) Vandonselaar, M.; Hickie, R. A.; Quail, J. W.; Delbaere, L. T. Trifluoperazine-induced conformational change in Ca(2+)-calmodulin. *Nature Struct. Biol.* **1994**, *1*, 795–801.
(30) Smith, P. K.; Krohn, R. I.; Hermanson, G. T.; Mallia, A. K.; Gartner, F. H.; Provenzano, M. D.; Fujimoto, E. K.; Goeke, N. M.; Olson, B. J.; Klenk, D. C. Measurement of protein using bicinchoninic acid. *Anal. Biochem.* **1985**, *150*, 76–85.
(31) Wedemeyer, W. J.; Baker, D. Efficient minimization of angle-dependent potentials for polypeptides in internal coordinates. *Proteins* **2003**, *53*, 262–272.
(32) DeLano, W. L. Use of PYMOL as a communications tool for molecular science. *Abstr. Pap. Am. Chem. Soc.* **2004**, *228*, U313–U314.